ADVANCING EARTH AND SPACE SCIENCE

Water Resources Research

RESEARCH ARTICLE
10.1029/2020WR029529

Key Points:

- An analytical curve was established to depict the spatial variability of mean annual baseflow based on the Budyko "limit" framework
- The curve directly relates aridity index and storage capacity (Sp) to estimate baseflow and shows dominant control of Sp in humid catchments
- The developed curve performed well with observed data from 950 catchments located in the Australia, CONUS and UK

Supporting Information:

Supporting Information may be found in the online version of this article.

Correspondence to:

L. Cheng,
lei.cheng@whu.edu.cn

Citation:

Cheng, S., Cheng, L., Liu, P., Qin, S., Zhang, L., Xu, C.-Y., et al. (2021). An analytical baseflow coefficient curve for depicting the spatial variability of mean annual catchment baseflow. *Water Resources Research*, *57*, e2020WR029529. https://doi.org/10.1029/2020WR029529

Received 28 DEC 2020
Accepted 20 JUL 2021

An Analytical Baseflow Coefficient Curve for Depicting the Spatial Variability of Mean Annual Catchment Baseflow

Shujie Cheng[1,2,3], Lei Cheng[1,2,3], Pan Liu[1,2,3], Shujing Qin[1,2,3], Lu Zhang[4], Chong-Yu Xu[1,5], Lihua Xiong[1,2,3], Liu Liu[6], and Jun Xia[1,2,3]

[1]State Key Laboratory of Water Resources and Hydropower Engineering Science, Wuhan University, Wuhan, China, [2]Hubei Provincial Collaborative Innovation Center for Water Resources Security, Wuhan, China, [3]Hubei Provincial Key Lab of Water System Science for Sponge City Construction, Wuhan University, Wuhan, China, [4]CSIRO Land and Water, Black Mountain, Canberra, ACT, Australia, [5]Department of Geosciences, University of Oslo, Oslo, Norway, [6]College of Water Resources and Civil Engineering, China Agricultural University, Beijing, China

Abstract Catchment baseflow is jointly controlled by climate and landscape properties. Previous studies have recognized that spatial variability of mean annual baseflow coefficient (BFC = Q_b / P, ratio of baseflow to precipitation) is primarily controlled by aridity index and storage capacity. However, an analytical solution of BFC in terms of the dominant controlling factors has not yet been established. The objective of this study was to develop an analytical BFC curve to depict spatial variability of BFC based on the "limit" concept of the Budyko framework. The BFC curve relates the baseflow coefficient to aridity index and storage capacity without resolving complex interactions between evapotranspiration and baseflow generation. The proposed BFC curve showed that, in the arid catchments, baseflow coefficient was primarily limited by available water (precipitation, P) and, in the humid catchments, was jointly controlled by both the available energy (potential evapotranspiration, E_p) and catchment retention capability (ratio of catchment storage capacity to P, i.e., S_p/P). Observed hydrological data from 950 catchments in Australia, the conterminous United States and the United Kingdom with diverse hydro-climatic conditions (BFC = 0.001–0.650) were collected to demonstrate the capability of the developed curve. Results showed that the BFC curve captured the spatial variability of observed BFC in the 950 study catchments (R^2 = 0.75, RMSE = 0.058). Mean annual baseflow estimated by the BFC curve agreed well with observed baseflow (R^2 = 0.86, RMSE = 0.19 mm). The developed analytical curve provides an analytical solution for understanding how aridity index and storage capacity control mean annual catchment baseflow, and will improve predictability of baseflow at ungauged basins.

1. Introduction

Baseflow (Q_b) is the portion of streamflow that comes from groundwater and other delayed sources, and generally sustains river flows during dry periods (S. Cheng et al., 2020; Hall, 1968; Wu et al., 2019). Understanding how baseflow varies spatially with changing climate and landscape properties is crucial for dealing with various water resource management issues related to water quantity and quality such as sustaining aquatic habitats (Fan et al., 2013; Poff et al., 1997), water supply (Kelly et al., 2019; W. Xu et al., 2021), diluting pollution from wastewater (Male & Ogawa, 1984; Smakhtin, 2001), etc. At the mean annual scale, there is a general consensus that the spatial variability of baseflow is controlled by climate and catchment properties, including precipitation, potential evapotranspiration, soil, geology, topography, and vegetation (Mcdonnell et al., 2007). However, the identified dominant factors controlling baseflow have been different in different studies. These factors include precipitation and potential evapotranspiration (Ahiablame et al., 2013; Beck et al., 2013; Peña-Arancibia et al., 2010; Van Dijk, 2010), geology, topography, and soil properties (Bloomfield et al., 2009; Brandes et al., 2005; Gebert et al., 2007; Jolánkai & Koncsos, 2015; Longobardi & Villani, 2008; Rumsey et al., 2015; Singh et al., 2019), and vegetation (L. Cheng et al., 2017; Huseby Karlsen et al., 2016). A universal method for explaining the underlying mechanisms of climate and physiography that control the spatial variability of baseflow is still lacking (Price, 2011).

Catchment storage capacity plays a major role in how much precipitation will be partitioned into baseflow, especially in humid catchments (Gnann et al., 2019). In humid catchments with saturation-excess mechanisms, storage capacity determines how much precipitation becomes surface runoff (Q_s) or soil wetting retention (Milly, 1994; Sankarasubramanian & Vogel, 2002; Yokoo et al., 2008). For catchment with small retention capability, storage capacity can be easily and frequently filled up and become saturated, with a larger fraction of precipitation quickly becoming runoff as saturated surface flow to the stream and lesser baseflow generated (Hahm, Rempe et al., 2019). However, very few studies have used the storage capacity to directly depict the spatial variability of baseflow. Aridity index (AI, commonly embedded in the Budyko (1958, 1974)) is generally considered to be the dominant control on hydrological partitioning, while catchment storage capacity is usually regarded as being much less important (Abatzoglou & Ficklin, 2017; Trancoso et al., 2016; X. Xu et al., 2013). Wang and Wu (2013) attempted to use aridity index as a first order controlling factor on baseflow, assuming that baseflow coefficient (i.e., BFC = Q_b / P) has similar behavior as the total flow coefficient (i.e., TFC = Q/P). Neto et al. (2020) also reported that the spatial variability of baseflow can be captured using an exponential function of aridity index only. Based on a data set that included humid catchments in the United Kingdom, Gnann et al. (2019) recognized that storage capacity was as important as aridity index and was a first-order control on spatial variability of BFC in humid catchments. In Gnann et al. (2019), the numerical solution of BFC derived from the Ponce-Shetty model (Ponce & Shetty, 1995; Sivapalan et al., 2011) was too complex to aid understanding of the upper limit control of storage capacity on baseflow generation. Except Wang (2018) proposed an analytical expression of total runoff as a function of storage capacity and wetness, a simple equation to directly relate storage capacity to mean annual baseflow estimation has not yet been found (Neto et al., 2020).

The spatial variability of mean annual total flow can be well formulated by the Budyko framework (Budyko, 1974; Fu, 1981; Good et al., 2017; Shen et al., 2017; Yang et al., 2007; L. Zhang et al., 2004). The "limit" concept of the Budyko framework is a useful tool for dealing with spatial variability issues as it provides two theoretical upper bounds under equilibrium conditions (Calder, 1998; Good et al., 2017; L. Zhang et al., 2008). The Budyko framework shows that, under very dry conditions, evapotranspiration (E_a) is limited by available water supply (P), and under very wet conditions, E_a is limited by available energy demand (E_p). However, a similar framework that incorporates the "limit" of storage capacity to show the spatial variability of baseflow has not been reported in the literature (Neto et al., 2020). Most of the previous studies that have attempted to depict the spatial variability of BFC usually partitioned precipitation into baseflow using two-step methods in terms of temporal runoff generation processes following rainfall events at the point scale, such as the Lvovich approach (Lvovich, 1979) and the Ponce-Shetty model (Ponce & Shetty, 1995; Sivapalan et al., 2011). The two-step partitioning methods must detangle the interactions amongst E_a, Q_s, and Q_b both temporally (step-by-step at the annual or monthly scale) and spatially (between catchments). These methods consider baseflow and evapotranspiration as complementary components partitioned from soil wetting, and results in the controlling factors for baseflow to be complex and unclear (Gnann et al., 2019; Sivapalan et al., 2011; Tang & Wang, 2017). L. Zhang et al. (2008) suggested that the "limit" concept for total flow (Q) (i.e., Budyko framework) could be extended to depict the surface flow (Q_s) generation between catchments by introducing storage capacity as another theoretical boundary. It is well known that mean annual catchment Q_b can be estimated by subtracting Q_s from Q (i.e., $Q_b/P = Q/P - Q_s/P$). If the "limit" hypothesis for Q_s proposed by L. Zhang et al. (2008) is valid, then the combination of the Budyko framework for Q/P and the extended Budyko framework for Q_s/P can relate Q_b/P to climatic factors and storage capacity. We can thus focus only on spatial variability without having to resolve complex interactions between evapotranspiration and baseflow generation.

To depict the spatial variability of baseflow, an analytical framework (i.e., BFC curve) was developed by combining the Budyko framework (for Q/P) and the extended Budyko framework (for Q_s/P) that accounts for the dominant controls of both aridity index and storage capacity on baseflow coefficient (BFC). Observed hydro-meteorological data for 950 catchments across Australia, the conterminous United States, and the United Kingdom with a wide range of climatic and physiographical conditions are collected to test the capability of the proposed BFC curve. Furthermore, catchment storage capacity is inferred from the Ponce-Shetty model due to the lack of directly observed values. The primary objectives of this study were to (1) determine if storage capacity is as important to baseflow as aridity index is; (2) develop an analytical BFC curve to depict the spatial variability of baseflow by directly relating storage capacity and aridity index to baseflow estimation; (3) examine the capability of the developed BFC curve using observed baseflow coefficients for 950 study catchments.

10.1029/2020WR029529

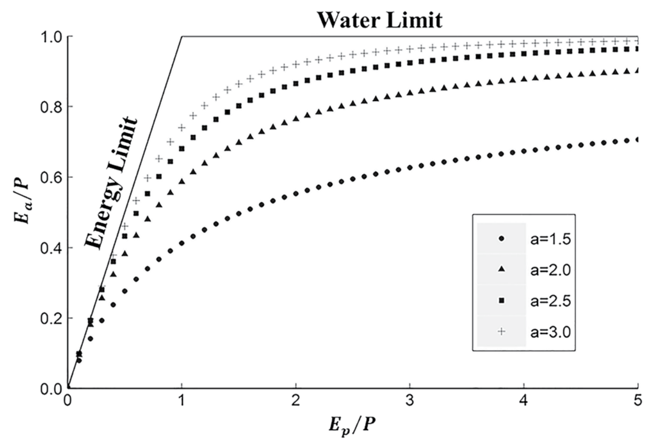

Figure 1. Schematic diagram of Budyko framework for partitioning mean annual precipitation (P) into actual evapotranspiration (E_a) and runoff based on the "limit" concept. E_p is potential evapotranspiration.

2. Derivation of Baseflow Coefficient Curve

2.1. "Limit" Concept in Budyko Framework

The Budyko framework can partition long-term precipitation into runoff (Q) and actual evapotranspiration (E_a) by considering only the dominant controls of water supply (typically P) and energy demand (typically E_p) on E_a (Budyko, 1958; L. Cheng et al., 2011; Good et al., 2017). As shown in Figure 1, the "limit" concept (the fundamental theory of the Budyko framework) places two theoretical limit boundaries on E_a (Good et al., 2017; L. Zhang et al., 2008). Mathematically, the "limit" concept can be expressed as:

$$E_a \,/\, P \rightarrow 1 \quad \text{as}\, E_p \,/\, P \rightarrow \infty \quad \left(\text{for very dry conditions}\right) \tag{1}$$

$$E_a \rightarrow E_p \quad \text{as}\, E_p \,/\, P \rightarrow 0 \quad \left(\text{for very wet conditions}\right) \tag{2}$$

that is, under very dry conditions when evapotranspiration is limited by water supply, E_a will approach P; and under very wet conditions when evapotranspiration is limited by energy demand, E_a will asymptotically approach E_p.

The "limit" concept for evapotranspiration can be appropriately applied to catchment rainfall retention (CR). When catchment P is partitioned into Q_s and CR (i.e., $P = Q_s + CR$), L. Zhang et al. (2008) proposed that CR satisfies the extended "limits" concept, and is defined as:

$$CR \,/\, P \rightarrow 1 \quad \text{as}\, CR_0 \,/\, P \rightarrow \infty \quad (\text{for very dry conditions}) \tag{3}$$

$$CR \rightarrow CR_0 \quad \text{as}\, CR_0 \,/\, P \rightarrow 0 \quad \left(\text{for very wet conditions}\right) \tag{4}$$

where the demand limit for CR is CR_0 (the sum of soil storage capacity S_p and potential evapotranspiration E_p). The supply limit for CR is considered to be P. CR_0/P is analogous to Budyko's aridity index (E_p/P).

2.2. Derivation of BFC Curve Based on the "Limit" Concept

An analytical framework (i.e., BFC curve) was developed in this study to depict the spatial variability of mean annual catchment baseflow. Based on the "limit" concept, both runoff coefficient (Q/P) and surface flow coefficient (Q_s/P) can be derived using the Budyko framework. As shown in Figure 2, baseflow coefficient (Q_b/P) is calculated as the difference between Q/P and Q_s/P.

Q/P can be calculated from E_a/P (i.e., $Q/P = 1{-}E_a/P$) under equilibrium conditions, that is, when storage change can be neglected. Based on the "limits" concept, E_a/P is calculated using the equation proposed by Fu (1981) (see Figure 1), which is one of the analytical models for estimating mean annual evapotranspiration (L. Zhang et al., 2004). Assuming that E_a/P satisfies a Budyko curve with a parameter a_1, Fu's equation can be expressed as:

$$\frac{E_a}{P} = 1 + \frac{E_p}{P} - \left[1 + \left(\frac{E_p}{P}\right)^{a_1}\right]^{1/a_1} \tag{5}$$

When change in catchment water storage can be neglected, one can obtain:

$$\frac{Q}{P} = -\frac{E_p}{P} + \left[1 + \left(\frac{E_p}{P}\right)^{a_1}\right]^{1/a_1} \tag{6}$$

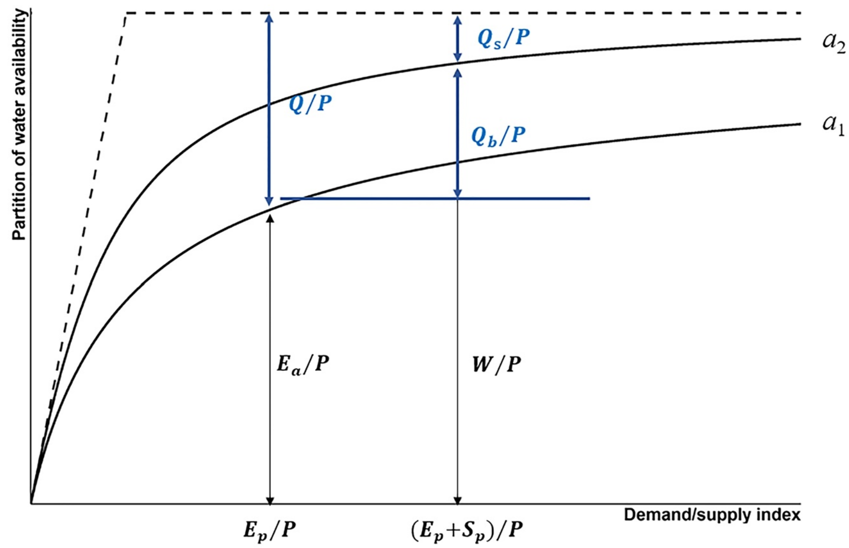

Figure 2. Schematic diagram showing partitioning baseflow (Q_b) from precipitation (P) combining first step and second step partitioning at the mean annual scale based on the "limit" concept. E_a is actual evapotranspiration, E_p is potential evapotranspiration, Q is total flow, Q_b is baseflow, Q_s is surface flow, W is catchment wetting, S_p is storage capacity, a_1 and a_2 are parameters.

where a_1 is a parameter representing the joint control of other secondary climatic and landscape properties on evapotranspiration efficiency. Parameter a_1 ranges from 1 to ∞. A higher a_1 indicates a larger evapotranspiration efficiency (i.e., higher actual evapotranspiration and lower runoff for a given precipitation and potential evapotranspiration condition).

Q_s/P is calculated as a function of catchment rainfall retention fraction (CR/P) (i.e., $Q_s/P = 1 - CR/P$). Similar to the calculation of E_a/P, the calculation of CR/P also uses the Budyko formulation proposed by Fu (1981) based on the "limit" concept (see Equations 3 and 4). Assuming that CR satisfies the Budyko curve with parameter equal to a_2, the mathematic equation for estimating CR/P is:

$$\frac{CR}{P} = 1 + \frac{E_p + S_p}{P} - \left[1 + \left(\frac{E_p + S_p}{P}\right)^{a_2}\right]^{1/a_2} \tag{7}$$

Then, Q_s/P is calculated from $1 - CR/P$, expressed as:

$$\frac{Q_s}{P} = -\frac{E_p + S_p}{P} + \left[1 + \left(\frac{E_p + S_p}{P}\right)^{a_2}\right]^{1/a_2} \tag{8}$$

where a_2 is a parameter representing the joint control of all other secondary climatic and landscape properties (except for storage capacity S_p) on retention efficiency. A larger a_2 value will result in more rainfall retention and less surface runoff. As stated earlier, S_p is effective catchment storage capacity, defined as the maximum water volume that a catchment can hold after rainfall events (McNamara et al., 2011; Pan et al., 2020).

Combining Equations 6 and 8, Q_b/P can be calculated from $Q/P - Q_s/P$ as:

$$\frac{Q_b}{P} = \frac{S_p}{P} + \left[1 + \left(\frac{E_p}{P}\right)^{a_1}\right]^{1/a_1} - \left[1 + \left(\frac{E_p + S_p}{P}\right)^{a_2}\right]^{1/a_2} \tag{9}$$

Under very limited storage capacity conditions (for instance, an impervious catchment), the available water for baseflow generation approaches 0, and baseflow also approaches 0, that is,

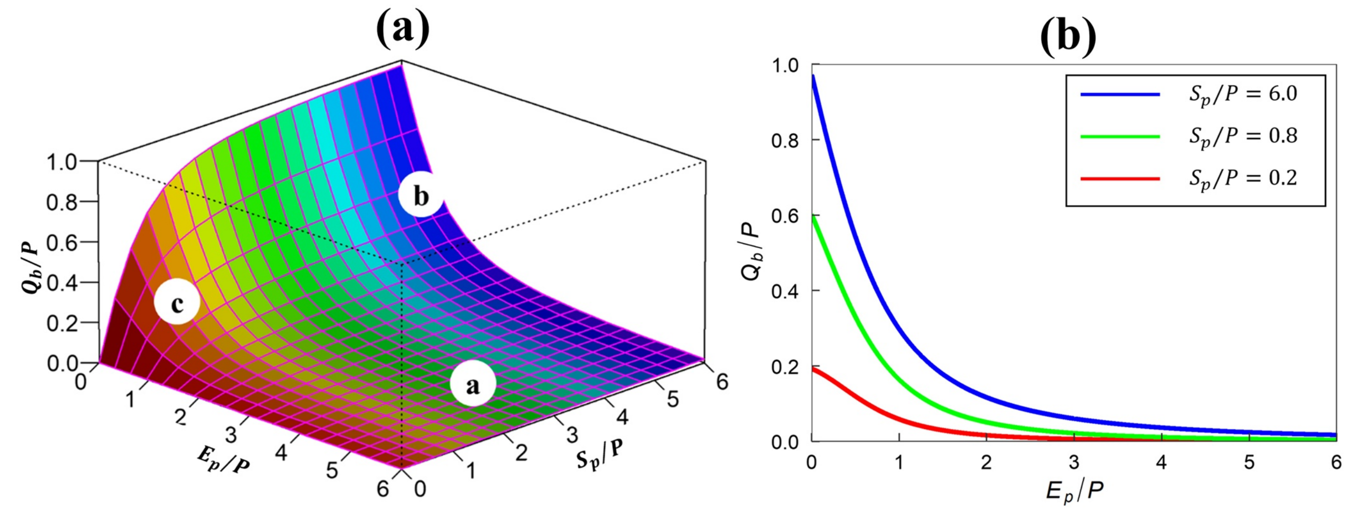

Figure 3. Visualization of the developed baseflow coefficient curve (i.e., Equation 11): (a) 3-dimensional state space and (b) 2-dimensional Q_b/P versus E_p/P space in which S_p/P is left as a parameter. Subregions (a–c) in panel (a) represent different catchment conditions. Note that the color of the state space has no meaning, but is provided for better visualization. Q_b is baseflow, P is precipitation, E_p is potential evapotranspiration, S_p is storage capacity.

$$Q_b / P \to 0 \quad \text{as } S_p / P \to 0 \tag{10}$$

Therefore, when $E_p + S_p/P$ approaches E_p/P (i.e., $S_p/P \to 0$), Q_s/P should approach Q/P to make $Q_b/P \to 0$ (see Figure 2). To satisfy this boundary condition, parameter a_1 has to be equal to parameter a_2. Thus Equation 9 can be written as:

$$\frac{Q_b}{P} = \frac{S_p}{P} + \left[1 + \left(\frac{E_p}{P}\right)^{\alpha}\right]^{1/\alpha} - \left[1 + \left(\frac{E_p + S_p}{P}\right)^{\alpha}\right]^{1/\alpha} \tag{11}$$

where α is a new lumped parameter, reflecting the secondary controls of other climatic and landscape properties on long-term baseflow generation. These other properties include vegetation, slope, elevation, and soil infiltration capacity, etc. α ranges from 1 to ∞. This simplification has a limitation that a_1 and a_2 reflect joint control of secondary climatic and landscape properties on Q/P and Q_s/P, respectively. The simplification $a_1 = a_2$ is adopted in this study to satisfy the boundary condition (i.e., Equation 10) and to obtain a simple formulation to be shown in 3D space as in Figure 3a. Furthermore, the influence of the simplification $a_1 = a_2$ on the shape of the BFC curve is unnoticeable because both a_1 and a_2 reflect the secondary controls on baseflow. The influence of α on baseflow coefficient will be discussed in Section 5.3.

The BFC curve specifies that Q_b/P is a function of aridity index (E_p/P) and S_p/P, where S_p/P is defined as the retention index. The sum of E_p/P and S_p/P represents catchment capability to retain mean annual precipitation for baseflow and evapotranspiration. P, E_p, and S_p are the dominant factors that determine how much precipitation will be partitioned into baseflow.

2.3. Visualization of the Developed BFC Curve

Figure 3a shows the 3-dimensional (3D) state space of the developed BFC curve (Equation 11). Catchment aridity index (E_p/P) and the retention index (S_p/P) have opposite effects on how much precipitation becomes baseflow at mean annual scale. BFC decreases nonlinearly with increasing E_p/P, but increases nonlinearly with increasing S_p/P. The joint controls of E_p/P and S_p/P are demonstrated using several BFC curves in Figure 3a. Figure 3b shows the projection of 3D BFC curves into Q_b/P versus E_p/P 2-dimensional (2D) space, and clearly shows the influence of S_p/P on catchment BFC. The 2D BFC curves in Figure 3b are similar to the shape of the Budyko curves for Q/P and Q_b/P (both decreasing with increasing E_p/P). The difference is that BFC curves have different values when E_p/P approaches 0. For curves with very large re-

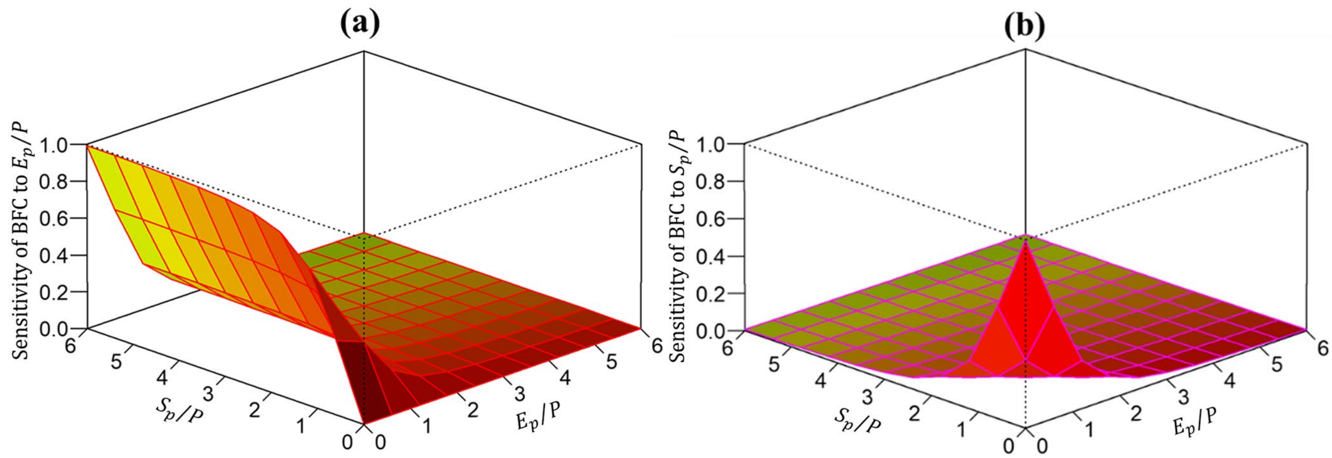

Figure 4. Sensitivity of baseflow coefficient (BFC $= Q_b\ /\ P$) to the dominant control factors: (a) the sensitivity to aridity index (E_p/P) and (b) the sensitivity to retention index (S_p/P). Note that the color of the state space has no meaning but is provided for better visualization. P is precipitation, E_p is potential evapotranspiration, S_p is storage capacity.

tention index (e.g., $S_p/P = 6.0$), BFC approaches 1.0 when $E_p/P = 0$, and then decreases with increasing E_p/P. BFC for curves with very small retention index (e.g., $S_p/P = 0.2$) are much smaller than 1.0 when $E_p/P = 0$. The different shapes of BFC curves indicate that the controls of aridity index and retention index on BFC are different across different catchment conditions.

Basically, the state space of the BFC curve can be divided into three subregions, that is, (a–c) regions in Figure 3a, according to the relative importance of the three limits (P, E_p, and S_p) on BFC across different conditions. Subregion (a) represents the precipitation-limited condition with small P and large E_p ($E_p/P \geq 1.0$ as suggested by Fu, 1981). Subregion (b) represents the energy-limited condition with small E_P, large P, and large S_p ($E_p/P < 1.0$, $S_p/P \geq 5.0$, note that the sensitivity of BFC to S_p/P is equal to 0 when $S_p\ /\ P = 5.0$ [see Figure 4b]). Subregion (c) represents the combination of energy- and storage-capacity-limited conditions with small E_p, small S_p, and large P ($E_p/P < 1.0$, $S_p/P < 5.0$). In the precipitation-limited and energy-limited conditions in subregions (a and b), E_p/P has a much more dominant influence than S_p/P on BFC. In subregion (c), baseflow is jointly controlled by energy and storage capacity, and both S_p/P and E_p/P have significant impacts on BFC.

The impacts of E_p and S_p in subregion (c) can be further demonstrated by the sensitivity of BFC to E_p/P and S_p/P (see Figure 4). BFC is sensitive to changes in E_p/P at low E_p/P, and sensitivity increases with increasing S_p/P (Figure 4a). BFC is sensitive to changes in S_p/P only at low E_p/P and low S_p/P conditions (Figure 4b). At low E_p/P and low S_p/P conditions (i.e., subregion (c)), the response of BFC to both E_p/P and S_p/P indicates that both E_p and S_p are important for depicting the spatial variability of BFC in humid catchments.

From Figures 3 and 4, it can be seen that aridity index is the dominant control on BFC in all conditions, while retention index has significant impact on BFC only in humid catchments with small retention index where typically $E_p/P < 2.0$ and $S_p/P < 2.0$. Mean annual catchment baseflow is determined by three first order controls, water supply P, energy demand E_p and catchment storage capacity S_p. When S_p is smaller than P, S_p can be easily and frequently saturated for baseflow generation. Under this condition, a large fraction of P runs off quickly to the stream as surface flow rather than baseflow. Compared with the first order controls of P and E_p in the Budyko framework, the introduction of S_p as a first order factor as important as P and E_p for baseflow generation is the fundamental characteristic of the BFC curve.

3. Catchments and Data

Daily hydrological and meteorological data from a total of 950 catchments were used to test the capability of the developed analytical baseflow coefficient curve. These 950 catchments were located in Australia ($n = 443$), the conterminous United States ($n = 372$), and the United Kingdom ($n = 135$).

3.1. Australian Catchments and Data

Long-term daily precipitation, potential evapotranspiration and streamflow data of 443 un-nested catchments in Australia were obtained. Data for these catchments are part of the Australia unregulated catchment data set (Y. Zhang et al., 2013) with minimum instances of human interference (i.e., without dams, intensive irrigation, and land use change). Daily catchment precipitation and potential evapotranspiration were aggregated from the 5 km gridded data set. Gridded daily meteorological data including precipitation, temperature, solar radiation and vapor pressure were provided by the Australian Bureau of Meteorology (BoM) (http://www.bom.gov.au/climate/data/). Gridded potential evaporation was calculated by the Priestley-Taylor equation (Priestley & Taylor, 1972) using BOM meteorological data and 5 km monthly albedo data created using 1 km resolution MODIS albedo data (https://modis.gsfc.nasa.gov/). The collected precipitation, streamflow and potential evapotranspiration data in Australia span over the period of 1975–2012. All the catchments have a minimum length of 20-years records with at least 10-years continuous records and less than 10% missing data in total. The drainage area ranged from 48 to 72,902 km^2. These 443 catchments have a broad range of hydrological characteristics. The average precipitation is 948 mm ± 413 (mean ± standard deviation), aridity index is 1.76 ± 1.01, runoff coefficient is 0.19 ± 0.15, and baseflow coefficient is 0.06 ± 0.07.

3.2. Conterminous United States Catchments and Data

A total of 372 catchments from the conterminous United States (CONUS) were used in this study, which are obtained from the Model Parameter Estimation Experiment (MOPEX) data set (Duan et al., 2006). Daily precipitation, potential evapotranspiration and streamflow data of these 372 catchments are collected, spanning the period of 1943–2003. The daily precipitation data sets were developed by the NWS Hydrology Laboratory (HL) based on rain gauge data from the National Climate Data Center (NCDC) (http://www.ncdc.noaa.gov/). The climatic potential evaporation data was derived from the NOAA Freewater Evaporation Atlas (Farnsworth et al., 1982), using the Penman method (Penman, 1948). The fraction of precipitation falling as snow of the selected catchments is no larger than 0.2 to avoid the influence of snow on baseflow separation. The drainage area of the study catchments varied from 67 to 10,375 km^2. The selected catchments cover all major geological and climate regions in the CONUS. The average precipitation is 1,038 mm ± 335 (mean ± standard deviation), aridity index is 1.07 ± 0.64, runoff coefficient is 0.35 ± 0.17, and baseflow coefficient is 0.15 ± 0.09.

3.3. United Kingdom Catchments and Data

The 135 selected catchments in the United Kingdom are part of the UK Benchmark Network (UKBN2) (Harrigan et al., 2018). Hydro-meteorological data for these catchments was obtained from different sources. Daily precipitation data were obtained from the Center for Ecology & Hydrology–Gridded Estimates of Areal Rainfall (GEH-GEAR) (Tanguy et al., 2016). Daily streamflow data and catchment boundaries were obtained from the website of National River Flow Archive (NRFA, 2019). Daily potential evapotranspiration data were obtained from the Climate Hydrology and Ecology Research Support System–Potential Evapotranspiration (GHESS-PE) (E. L. Robinson et al., 2017). The potential evapotranspiration were calculated using the Penman-Monteith equation for well-watered grass but a correction is added for interception on days where rainfall has occurred (Penman, 1948). Daily P and E_p data were at 1-km resolution and covered the period of 1986–2015 without any missing data. Available streamflow data length for these 135 catchments ranged from 24 to 87 years. The study period for the 135 catchments from the UK was set as the common period of the three data sets (1992–2015). The 135 study catchments in the UK were all in humid climatic conditions. The fraction of precipitation falling as snow of the selected UK catchments is no larger than 0.2. The average precipitation of all United Kingdom catchments is 1,254 mm ± 582 (mean ± standard deviation), aridity index is 0.51 ± 0.22, runoff coefficient is 0.59 ± 0.23, and baseflow coefficient is 0.25 ± 0.14.

3.4. Baseflow Separation

Daily baseflow (Q_b) and surface flow (Q_s) are separated from daily total streamflow (Q) using a digital filter technique, that is, the Lyne-Hollick (denoted as LH) method (Lyne & Hollick, 1979). Different digital filter techniques have no significant influence on the annual and mean annual estimation of Q_b and Q_s (L. Cheng et al., 2012, 2016; Kelly et al., 2019; Tan et al., 2020; J. Zhang et al., 2017). The LH method has the advantage of being minimally parameterized, and thus is easily applied to a large sample of catchments (Jolánkai & Koncsos, 2015). Here the LH method was applied in a traditional way, that is, baseflow was separated from total flow with three passes (forward, backward, and forward) and the filter parameter f_1 was set to 0.925 as suggested by Nathan and McMahon (1990). Daily Q_b and Q_s were aggregated to the annual and mean annual scales as observed Q_b and Q_s. Catchment baseflow coefficient (BFC) is calculated as the ratio of mean annual Q_b to mean annual P, that is, BFC = Q_b/P.

3.5. Estimation of Effective Storage Capacity S_p

Equation 11 has four parameters for estimation of mean annual catchment baseflow coefficient (BFC). One is a synthetic parameter (i.e., α), and the other three have explicit physical meanings (i.e., P, E_p, and S_p). P and E_p can be derived directly from long-term meteorological data, however, S_p is currently not available (Han et al., 2020). In this study, catchment effective storage capacity S_p was inferred from the process-based annual Ponce-Shetty model (Ponce & Shetty, 1995). This model is based on the two-stage partitioning theory of Lvovich (1979) that was later reintroduced by Sivapalan et al. (2011). The Ponce-Shetty model describes how precipitation is stored and released through the two-stage partitioning processes. The parameter wetting potential (W_p) in the Ponce-Shetty model was used to represent effective catchment storage capacity. W_p can well discriminate the difference in S_p between catchments in the following application and demonstration of Equation 11.

The two-stage partitioning theory partitions annual precipitation (P) into three components: surface flow (Q_s), baseflow (Q_b), and actual evapotranspiration (E_a). In the first stage, P is partitioned into Q_s and catchment wetting (W). In the second stage, W is further partitioned into Q_b and E_a. In the first stage partitioning, P=Q_s+W:

$$P < \lambda_s W_p, Q_s = 0, W = P \tag{12}$$

$$P < \lambda_s W_p, Q_s = \frac{\left(P - \lambda_s W_p\right)^2}{P + \left(1 - 2\lambda_s\right)W_p}, W = P - \frac{\left(P - \lambda_s W_p\right)^2}{P + \left(1 - 2\lambda_s\right)W_p} \tag{13}$$

$$P \to \infty, Q_s \to P - W_p, W \to W_p \tag{14}$$

In the second stage partitioning, $W = Q_b + E_a$:

$$W < \lambda_u V_p, Q_b = 0, E_a = W \tag{15}$$

$$W > \lambda_u V_p, Q_b = \frac{\left(W - \lambda_u V_p\right)^2}{W + \left(1 - 2\lambda_u\right)V_p}, E_a = W - \frac{\left(W - \lambda_u V_p\right)^2}{W + \left(1 - 2\lambda_u\right)V_p} \tag{16}$$

$$W \to \infty, Q_b \to W - E_a, E_a \to V_p \tag{17}$$

where W_p, V_p, λ_s, and λ_u are four parameters. W_p and V_p are the upper bounds on W and E_a, and are referred as the wetting and evapotranspiration potentials of a catchment, respectively. A higher value of W_p usually means a larger catchment storage capacity. A higher V_p usually means a larger potential evaporation rate. λ_s represents the proportion of P that must satisfy W before Q_s can occur. λ_u represents the proportion of W that must be used to satisfy E_a before baseflow Q_b can occur. λ_s and λ_u are coefficients related to the generation of surface flow and baseflow and have a range of $0 < \lambda_s, \lambda_u < 1$. The closer that λ_s and λ_u approach 1.0, the more difficult it is for a catchment to generate surface flow and baseflow, respectively.

W_p, V_p, λ_s, and λ_u in the Ponce-Shetty model were calibrated in every catchment using an automatic optimization technique (Genetic Algorithm (GA)) (Grefenstette, 1986) to maximize the Nash-Sutcliffe efficiency (Nash & Sutcliffe, 1970) of annual surface flow (NSE$_1$) and annual baseflow (NSE$_2$), stage by stage. Annual

Q_b and Q_s derived in Section 3.4 were used to calibrate annual parameters for the Ponce-Shetty model. W_p and λ_s were calibrated for the first stage by maximizing NSE_1 between "observed" Q_s separated from total streamflow using the LH method and Q_s simulated by the Ponce-Shetty model. V_p and λ_u for the second stage were calibrated by maximizing the NSE_2 between "observed" Q_b derived from the LH method and Q_b simulated by the Ponce-Shetty model. The influence of W_p on the partitioning process gives us insight into the control of storage capacity on the spatial variability of baseflow (Gnann et al., 2019). Therefore, the calibrated values of W_p for every catchment were further used to represent different magnitudes of catchment storage capacity (i.e., S_p) in the proposed method.

4. Validation of the Proposed BFC Curve

4.1. Maps of Flow Metrics and Catchment Climatic and Storage Attributes

Figure 5 shows the spatial distribution of observed total flow coefficient (TFC $= Q / P$) (Figure 5a), baseflow coefficient (BFC $= Q_b / P$) (Figure 5b), aridity index (AI $= E_p / P$) (Figure 5c) and retention index (S_p/P) (Figure 5d) across Australia, the conterminous United States, and the United Kingdom. Generally, BFC and TFC exhibited similar spatial patterns with higher values in the UK, lower values in Australia, and high variability in the CONUS. In Australia, the average TFC and BFC were 0.19 ± 0.15 (mean $\pm$ standard deviation) and 0.06 ± 0.07, respectively. Basically, BFC and TFC increased from inland to coastal catchments, especially in the southeast region within mainland Australia. In contrast, this was not the case for Western Australia, where BFC was relatively small even for the catchments close to the coast. In the CONUS, the average TFC and BFC were 0.35 ± 0.17 and 0.15 ± 0.09, respectively. Generally, TFC and BFC were smaller in the central and southeastern coastal regions than in other regions of the CONUS. TFC and BFC of most catchments located in the central CONUS were lower than 0.25 and 0.10, respectively. TFC and BFC became larger in the western CONUS. In the UK, the average TFC and BFC values were 0.58 ± 0.23 and 0.25 ± 0.14, respectively. Generally, TFC and BFC were smaller on the southeastern coast of the UK than in other regions. Except for the southeastern coast, TFC and BFC of most catchments were higher than 0.49 and 0.25, respectively. These results show that TFC and BFC are spatially distinct across catchments with different climate and landscape properties.

Generally, Aridity index (AI) was relatively smaller across the United Kingdom (humid region) than across the other two countries. Spatial variability of AI for CONUS catchments was greater than for the other two countries. The average AI in Australia, the CONUS, and the UK was 1.76 ± 1.01 (mean $\pm$ standard deviation), 1.07 ± 0.63, and 0.51 ± 0.22, respectively. The retention index (S_p/P) for the UK catchments were smaller than observed for the catchments in Australia and the CONUS. S_p/P showed no obvious spatial pattern for any of the three study countries. Generally, baseflow coefficient (BFC) and aridity index (AI) had oppositional spatial patterns across Australia and the CONUS. That is, higher AI values usually corresponded to lower BFC and vice versa (see Figures 5b and 5c). However, this oppositional spatial pattern was not obvious across the United Kingdom.

4.2. Joint Control of Aridity Index and Retention Index on Spatial Variability of Catchment Baseflow

Figure 6 shows scatter plots of total flow coefficient (Q/P) versus aridity index (E_p/P) (Figure 6a), as well as baseflow coefficient (Q_b/P) versus aridity index (E_p/P) (Figure 6b) for all 950 study catchments. Q/P decreases with the increases of E_p/P, falling relatively close to a single Budyko curve as expected. In contrast, Q_b/P did not always decrease with increasing E_p/P, and exhibited especially high variability in humid catchments located in the UK. Budyko curves (see Equation 6) were fitted for Q/P and Q_b/P by maximizing Nash-Sutcliffe efficiency (NSE; Nash & Sutcliffe, 1970) with parameter a equal to 2.6 and 6.9, respectively. Compared with NSE for observed Q/P and Budyko-simulated Q/P (0.81), the NSE of Q_b/P degraded remarkably (−0.76). This suggests that the Budyko curve was incapable of capturing the spatial variability of baseflow, especially the humid catchment located in the UK (see Figure S1). As interpreted by Gnann et al. (2019), the high variability of BFC in humid catchments shown in Figure 6b can be attributed to differences in catchment retention index S_p/P, indicating the influence of S_p/P on baseflow generation.

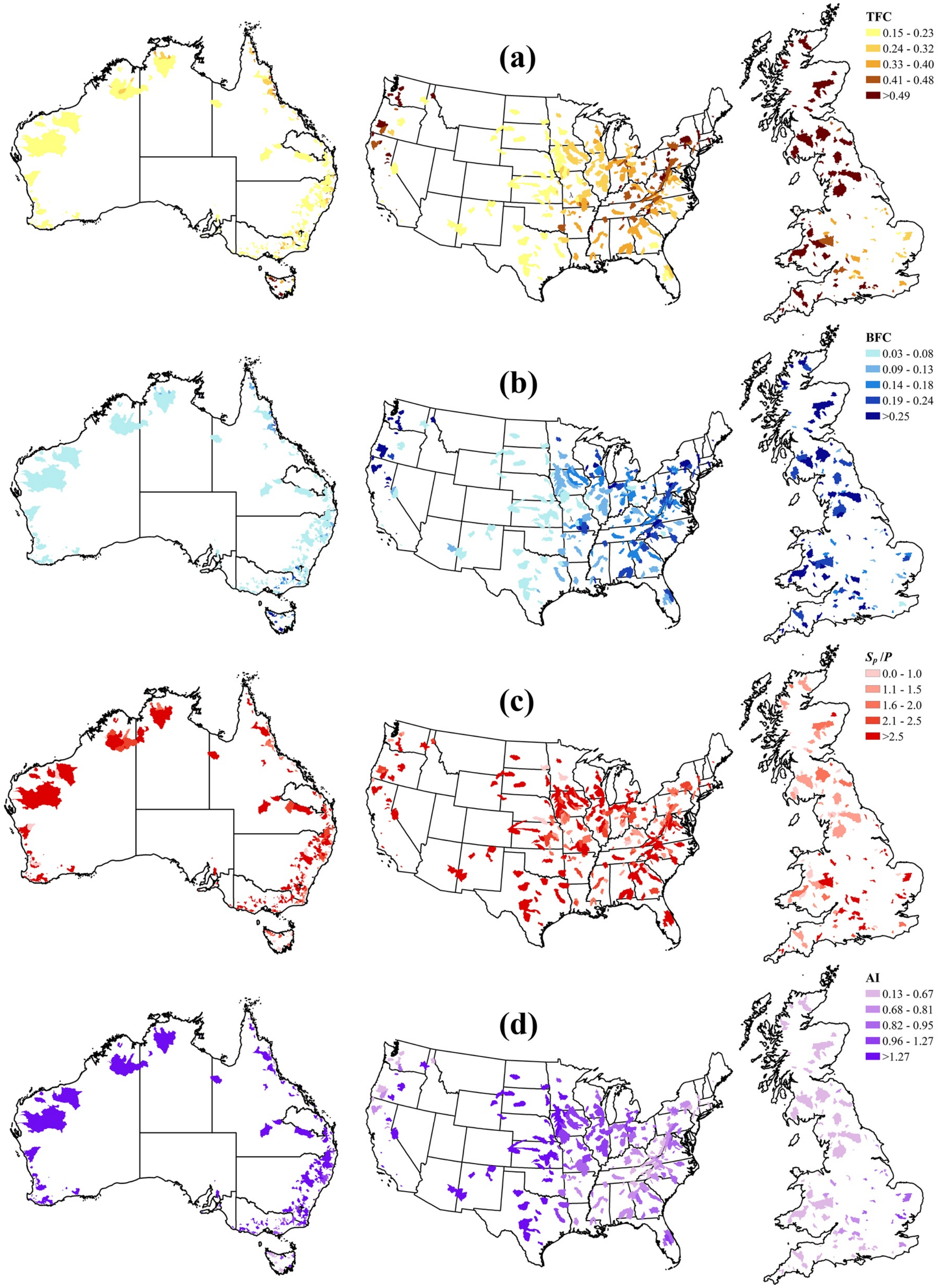

Figure 5. Spatial distribution of flow metrics and catchment attributes across Australia, the conterminous United States, and the United Kingdom: (a) total flow coefficient (TFC), (b) baseflow coefficient (BFC), (c) aridity index (AI), and (d) retention index (S_p/P). Note that the color scales of maps (a–d) are different. Note that the map scales are not the same in order to have better visualization.

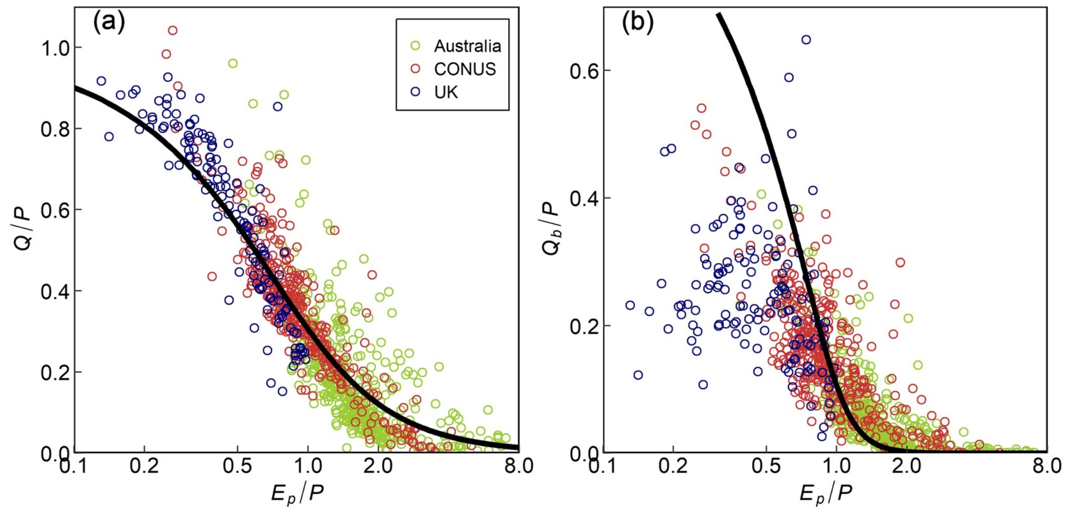

Figure 6. Plots relating flow coefficients to aridity index: (a) mean annual runoff coefficient (Q/P) versus aridity index (E_p/P) and (b) mean annual baseflow coefficient (Q_b/P) versus aridity index (E_p/P) across Australia (green circle), the conterminous United States (red circle), and the United Kingdom (blue circle). The black lines are the fitted Budyko curves with parameter α equal to 2.6 and 6.9, respectively. Q is total flow, Q_b is baseflow, P is precipitation, E_p is potential evapotranspiration.

As shown in Figure 7, scatterplots of observed Q_b/P versus E_p/P for all 950 catchments can be separated into three groups according to the magnitude of the surrogate retention index (S_p/P) (i.e., $S_p/P \leq 1.0$, $1.0 < S_p/P \leq 3.0$, and $S_p/P > 3.0$). The three separate point clouds demonstrate the great influence of S_p/P on Q_b/P. The point cloud with lowest S_p/P values exhibited lower BFC values (Figure 7a) and vice versa (Figure 7c). E_p/P and S_p jointly determined the spatial variability of catchment baseflow. Basically, 2D Q_b/P versus E_p/P BFC curves with different S_p/P values (similar lines shown in Figure 3b) can capture the observed BFC of the catchments (i.e., scatter points) in the three subplots of Figure 7. These results demonstrate that the joint control of aridity index and retention index on spatial variability of baseflow observed from catchment data can be depicted by the BFC curve proposed in this study.

4.3. Estimation of Baseflow Using Proposed BFC Curve

The 3-dimensional BFC curve (Equation 11) was used to estimate mean annual catchment BFC and baseflow. Aridity index (E_p/P) and retention index (S_p/P equal to W_p/P) of catchments are known values, and parameter α in Equation 11 was calibrated for each catchment using Genetic Algorithm (GA) (Grefenstette, 1986). The distribution of calibrated catchment α values is shown in the inset panel of Figure 8a. Because of the wide range of α values (1.0–4.0), the BFC curve using α fixed at 2.5 (i.e., median value of the range 1.0–4.0) cannot accurately model the observed BFC for all 950 catchments (Figure 8a). Thus, the 950 catchments were separated into three groups according to the calibrated α values, and shown in Figure 8b (α = 1.0–1.3, 430 catchments), Figure 8c (α = 1.31–3.0, 170 catchments), and Figure 8d (α = 3.01–4.0, 350 catchments). α values for the BFC curves were fixed at mean values of α for the three groups (i.e., 1.16, 1.77, and 3.83, respectively) to model catchment baseflow in the three separated groups shown in Figures 8b–8d, respectively. The state space for the three BFC curves appeared to cover the scatterplots of observed BFC well.

The simulated baseflow metrics using the BFC curve with α equal to 1.16, 1.77, and 3.83 were compared with the observed baseflow metrics in Figures 9a and 9b. The BFC curve estimated mean annual BFC and Q_b reasonably well compared with the observations. The coefficients of determination (R^2) and root mean square errors (RMSE) between the observed and simulated BFC were 0.75 and 0.058, respectively. The BFC curve also performed well in modeling Q_b, with R^2 and RMSE values of 0.86 and 0.19 mm, respectively. Furthermore, the BFC curve significantly improved the accuracy of Q_b/P and Q_b estimation compared with the Q_b/P and Q_b directly estimated by Budyko framework. Determination of Budyko parameter was consistent

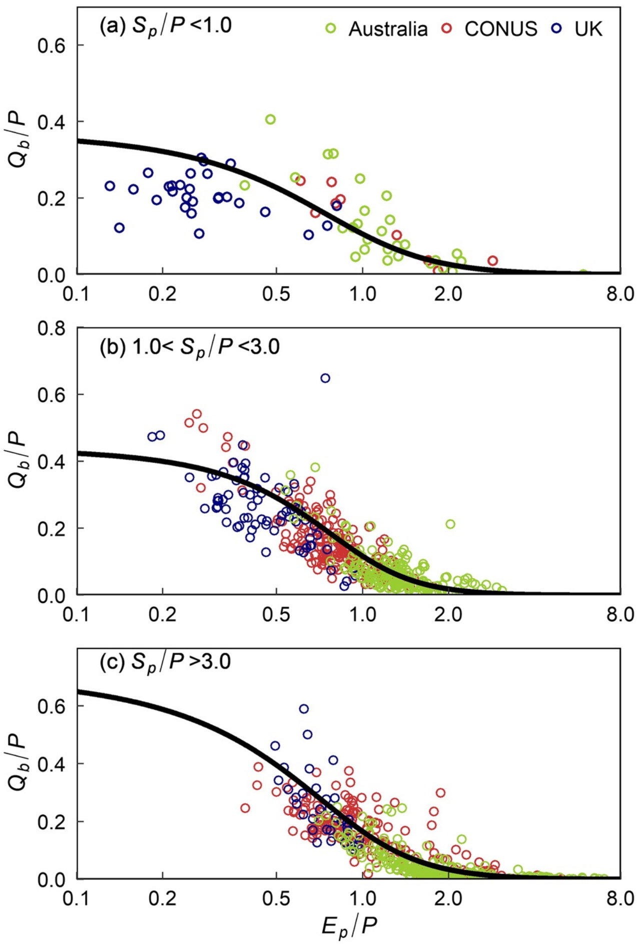

Figure 7. Scatterplots of observed baseflow coefficient (BFC = Q_b / P) versus aridity index (E_p/P) for 982 study catchments in Australia, the conterminous United States, and the United Kingdom. Each point represents one catchment at the mean annual scale. Three distinct point clouds separated by different ranges of S_p/P are presented, with (a) $S_p/P \leq 1.0$, (b) $1.0 < S_p/P \leq 3.0$, and (c) $S_p/P > 3.0$. The black lines in the figures are projected bidimensional BFC curves.

with that of BFC curve. The Budyko framework performed worse than the BFC curve with lower R^2 of 0.40 and 0.65 (Figure 9c), as well as larger RMSE of 0.087 and 0.30 mm for Q_b/P and Q_b estimation, respectively (Figure 9d). Figure 9 demonstrates that the proposed BFC curve determined in this study can accurately estimate mean annual catchment BFC and Q_b.

5. Discussion

5.1. Different Control of Storage Capacity on Q_b and E_a

Previous studies have reported the significant influence of storage capacity on hydrological partitioning (Donohue et al., 2012; Hahm, Dralle, et al., 2019; Shen et al., 2017). From a process-based perspective in the Ponce-Shetty model, storage capacity has a persistent effect on catchment wetting and catchment wetting simultaneously influences both baseflow and evapotranspiration. However, the influence of storage capacity on mean annual baseflow or spatial variability of baseflow are much more significant than the influence on evapotranspiration (Gnann et al., 2019; Neto et al., 2020). The different impact of storage capacity on Q_b and E_a can be well reflected in the BFC curve and the Budyko curve. In the Budyko framework, storage capacity is not a dominant controlling factor. Aridity index is the dominant factor controlling evaporation. For the baseflow coefficient, Equation 11 suggests that both the storage capacity and aridity index can affect baseflow significantly.

Although the structure of Ponce-Shetty model structure shows that storage capacity plays important roles in both baseflow and evaporation generation, the sensitivity analysis of the Ponce-Shetty model proves that storage capacity plays more important roles on Q_b than E_a. Figure 10 shows the sensitivity of Q_b and E_a to W_p in the Ponce-Shetty model. The relative changes of Q_b and E_a were calculated with the fitted parameter W_p changing by 40% (form −20% to 20%) in the 950 catchments. Q_b was much more sensitive to W_p than E_a, with the average relative change of Q_b being 35.4% ± 31.0% (mean ± standard deviation) and the average relative change of E_a being 7.4% ± 4.5% for all 950 study catchments. The relative change of Q_b was 3.9 ± 1.7 times larger than that of E_a. The much higher sensitivity of Q_b to W_p than E_a to W_p suggests that the influence of storage capacity on Q_b was much more important than the influence of storage capacity on E_a. It is reasonable that storage capacity is considered as a dominant control factor for Q_b in the BFC curve and a secondary control factor for E_a in the Budyko curve.

5.2. Advantages of Proposed Method for Estimating Long-Term Baseflow Coefficient

An important finding of this study is that the concise formulation of the BFC curve (Equation 11) can directly relate storage capacity to baseflow estimation. The simple but robust BFC curve mainly benefitted from the “limit” concept without detangling the complex interactions between evapotranspiration and baseflow generation temporally. Compared with conceptual models (e.g., the Ponce-Shetty model), the simple formulation of the BFC curve has advantages related to understanding how storage capacity affects baseflow.

Although the Ponce-Shetty model can represent detailed hydrologic processes and explicitly describe the controls of catchment properties on hydrological functions (Gentine et al., 2012; Potter et al., 2005), the complex numerical solution of BFC (Equation A1) based on the Ponce-Shetty model limits its practical application to explain the spatial variability of baseflow (Sivapalan et al., 2011; L. Zhang et al., 2001). Figure 11 shows the upscaled Ponce-Shetty model (described in the Appendix) at the mean annual scale to

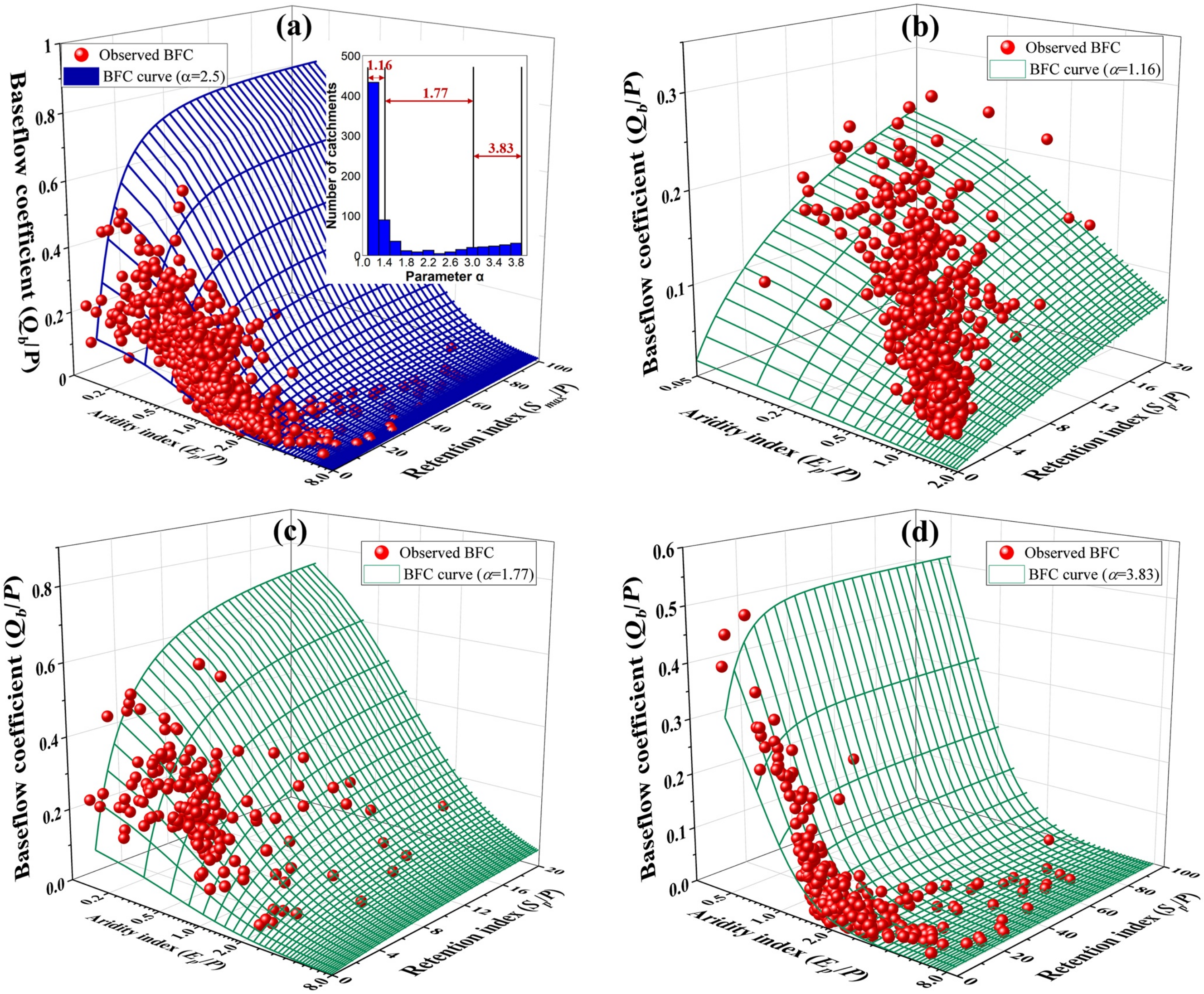

Figure 8. 3D plots of observed baseflow coefficients (BFC $= Q_b \ / \ P$) versus aridity index (E_p/P) and retention index (S_p/P): (a) all catchments and (b–d) catchments separated according to the value of parameter α. Each point represents one catchment at the mean annual scale. Lines are BFC curves with parameter α equal to (a) 2.5; (b) 1.16; (c) 1.77; and (d) 3.83. The inset panel (a) shows the distribution of calibrated catchment parameter α.

explain the spatial variability of observed BFC. The plot of observed BFC versus rescaled (see Appendix for description of rescaling) aridity index ($\widetilde{V_p} \ / \ \tilde{P}$) (Figure 11) is very similar to the BFC versus E_p/P plot (Figure 6). To some extent, the scatter points in Figures 11a can be roughly separated by rescaled precipitation ($\tilde{P}$). However, the plots cannot be separated by rescaled vapourization potential ($\widetilde{V_p}$) (Figures 11b). Essentially, the Ponce-Shetty model can symmetrically depict spatial variability in mean annual water balance (between-catchments) and temporal variability at the annual time scale (Gnann et al., 2019; Harman et al., 2011; Sivapalan et al., 2011). Regarding the spatial variability of mean annual catchment BFC, the upscaled Ponce-Shetty model at mean annual scale is too complex for explaining the spatial variability of mean annual baseflow because the rescaled aridity index ($\widetilde{V_p} \ / \ \tilde{P}$) is a synthesis of several factors including observed hydro-climate fluxes and four fitted parameters.

5.3. Secondary Controls on Proposed BFC Curve

The dominant controls of P, E_p, and S_p were explicitly accounted for in the proposed BFC curve. α in the proposed BFC curve represented the integrated secondary controls of catchment properties on the catchment

10.1029/2020WR029529

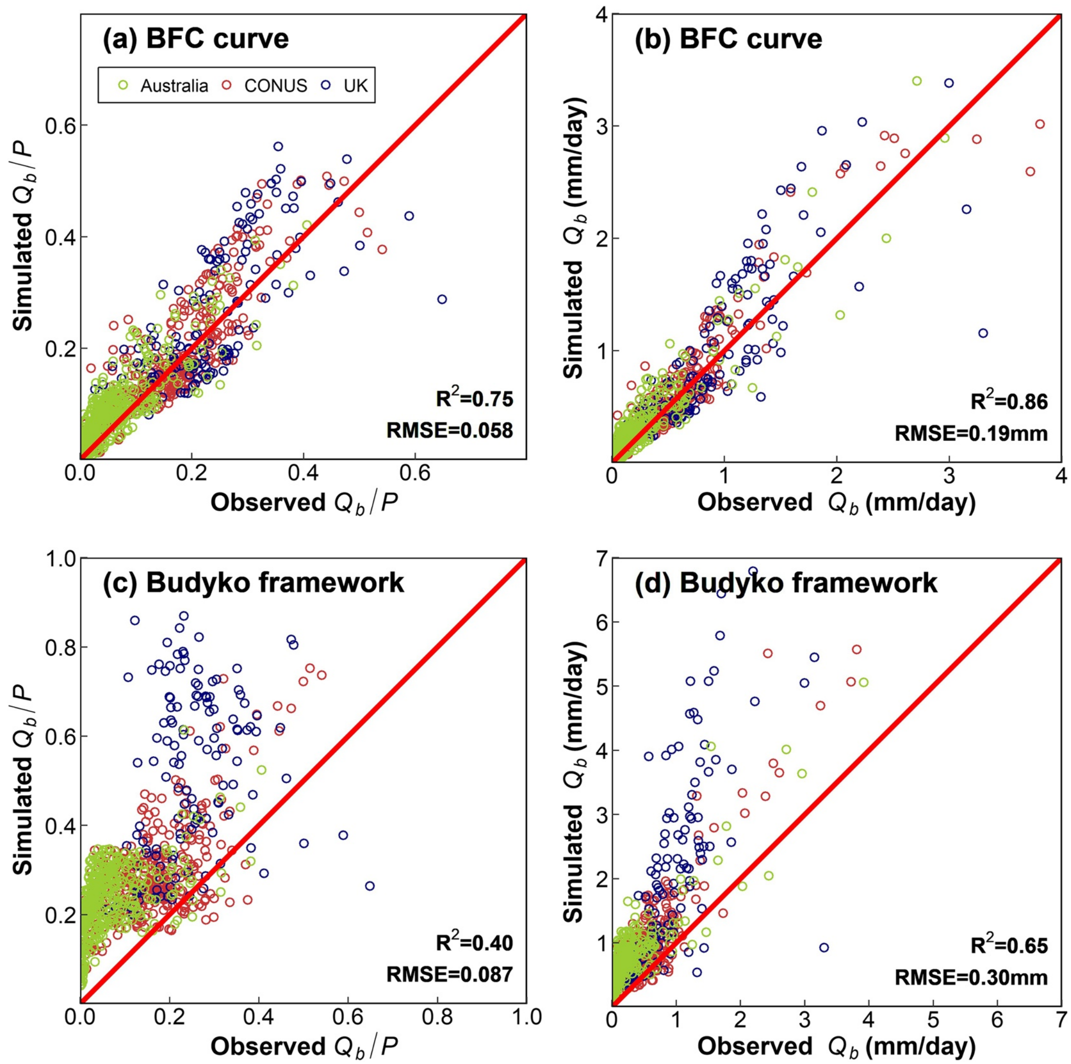

Figure 9. Scatterplots of observed and simulated baseflow metrics by baseflow coefficient curves (shown in Figure 8) and Budyko framework for 950 study catchments in Australia, the conterminous United States, and the United Kingdom: (a) baseflow coefficient (BFC = Q_b / P) estimated by BFC curve, (b) baseflow (Q_b) estimated by BFC curve, (c) Q_b/P estimated by Budyko framework, and (d) Q_b estimated by Budyko framework.

BFC. The larger the α value, the steeper the slope of the BFC curve. This means larger BFC in humid catchments and smaller BFC in arid catchments. For catchments with different properties, the value of α can be different. Figure 12 shows the spatial distribution of α calibrated in Section 5.3. Obvious spatial patterns of α can be seen across Australia and the conterminous United States. Basically, α was smaller on the southeast coast of Australia and became larger in western and northern Australia. α clearly increased from coastal to inland catchments in southeastern Australia. In the CONUS, α in western catchments had high variability. In the central CONUS, α had high values and became smaller in the eastern CONUS. In the UK, α for most catchments was small with α of 91.9% UK catchments smaller than 2.0.

The influences of all other secondary controlling factors are synthesized in parameter α, including intra-annual climate variability, soil, vegetation, and topography. Ahiablame et al. (2013) found that basin drainage area and open water bodies in the watershed were positively correlated with baseflow. Longobardi and Villani (2008) pointed out that permeability index influenced baseflow generation. Singh et al. (2019) evaluated the influence of catchment elevation, rain days, and upstream average slope on baseflow. It is essential to investigate the impact of the second controlling roles on α. The relationships between α and climate and landscape properties are also very important for advancing our understanding about the BFC curves, and

10.1029/2020WR029529

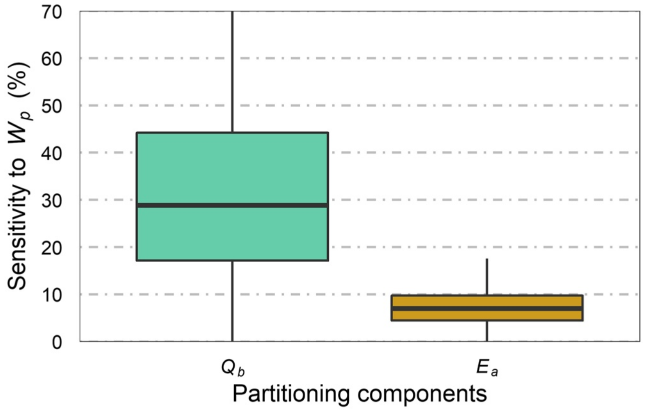

Figure 10. Boxplots of sensitivity of partitioning components (Q_b and E_a) to W_p using the Ponce-Shetty model. The *y*-axis values are the relative changes of Q_b and E_a with W_p changing by 40% (−20% to 20%). The lower and upper box boundaries indicate the 25th and 75th percentiles. The line inside the box indicates the median. Q_b is baseflow, E_a is evapotranspiration, W_p is wetting potential.

these relationships will be explored in the future with more data (Daly et al., 2019; Xing et al., 2018; X. Xu et al., 2013).

5.4. Implications of the Proposed BFC Curve

The assessment of the impacts of climate and vegetation changes on catchment water balance has a long tradition in hydrology. The Budyko framework has been widely used for analyzing the sensitivity of mean catchment water yield to the changes in aridity index, its individual components, and/or the lumped parameter (Roderick & Farquhar, 2011; Wang & Hejazi, 2011). Catchment baseflow can also be altered significantly by changing climate and vegetation (Ayers et al., 2019; Ficklin et al., 2016). Several studies have attempted to quantify the impact of climate and vegetation changes on baseflow through paired-catchment data (L. Cheng et al., 2017) and statistical analysis (Ahiablame et al., 2017; Tan et al., 2020; Trancoso et al., 2017). There is no analytical tool that can be used for such assessment, except for an exponential function of aridity index for baseflow modeling proposed by Meira Neto et al. (2020). However, this proposed method did not account for the control of storage capacity on baseflow, and the method was only tested using the conterminous United States catchments without considering the humid catchments in the United Kingdom. In this study, the proposed BFC curve was used for similar procedures as the Budyko framework, assessing the effects of climate change and storage capacity changes on spatial differences in baseflow and direct flow spatially. This method will likely prove valuable for studies of the effects of climate change on groundwater resources.

6. Conclusions

In this study, an analytical framework (i.e., baseflow coefficient curve; Equation 11), was developed to explain the spatial variability of baseflow coefficient (i.e., BFC $= Q_b \ / \ P$) using hydroclimatic data for 950 catchments across Australia, the conterminous United States, and the United Kingdom. By expressing BFC as a function of aridity index (E_p/P) and retention index (S_p/P), the BFC curve demonstrated that BFC decreased nonlinearly as E_p/P increased, and BFC increased nonlinearly as S_p/P increased. The BFC curve also

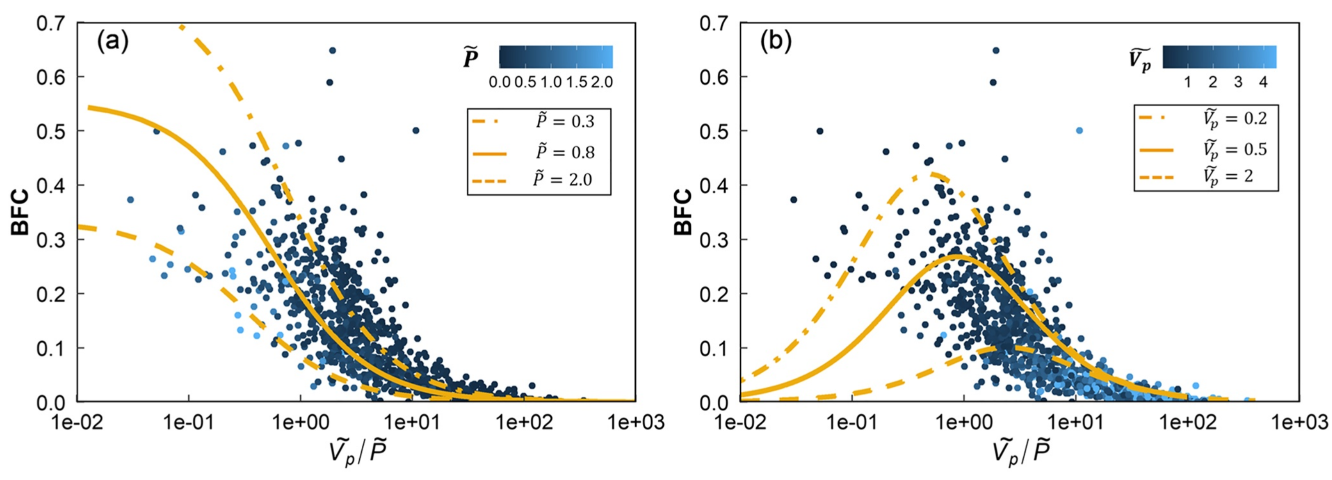

Figure 11. Scatterplots of observed baseflow coefficient (BFC $= Q_b \ / \ P$) versus rescaled aridity index ($\widetilde{V_p} \ / \ \tilde{P}$, see Ponce-Shetty model, Appendix) for 982 study catchments in Australia, the conterminous United States, and the United Kingdom. Each point represents one catchment at the mean annual scale. Lines are fitted Equation A1 derived from the Ponce-Shetty model. The scatterplots and lines are separated by different rescaled variables: (a) $\tilde{P}$ (rescaled precipitation) and (b) $\widetilde{V_p}$ (rescaled vapourization potential).

10.1029/2020WR029529

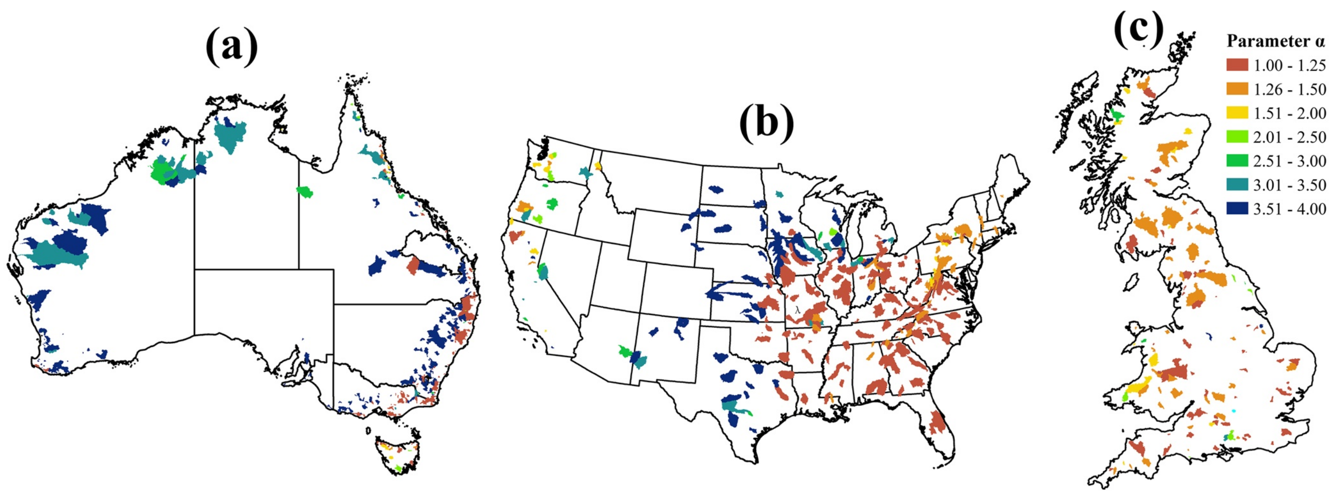

Figure 12. Spatial distribution of the calibrated parameter α across Australia, the conterminous United States, and the United Kingdom.

demonstrated that storage capacity is an important controlling factor on BFC as important as aridity index in humid catchments. Observed hydro-climate data for the 950 study catchments proved that the proposed BFC curve has excellent capability to capture the spatial variability of mean annual catchment baseflow. High variability of Q_b / P versus E_p / P scatterplots from humid catchments could be separated into three distinct point clouds according to S_p/P, consistent with the separation performed for BFC curves. Furthermore, the BFC curve performed well in modeling mean annual BFC for 950 study catchments with R^2 of 0.75 and RMSE of 0.058. The performance in modeling mean annual baseflow was good, with $R^2$of 0.86 and RMSE of 0.19 mm. The derived analytical BFC curve (Equation 11) in this study was used to predict the baseflow coefficient (Q_b/P) similar to how the Budyko equation predicts the runoff coefficient (Q/P). This method showed that both aridity index and storage capacity are the dominant controls on spatial variability of mean annual baseflow, thereby improving our ability to predict mean annual baseflow for ungauged catchments.

Appendix: Upscaled Ponce-Shetty Equations

The annual Ponce-Shetty model can be upscaled to the mean annual scale to model BFC. Based on the work of Sivapalan et al. (2011) and Gnann et al. (2019), BFC can be expressed as a function of rescaled climate variables:

$$\mathrm{BFC} = \frac{\tilde{P}}{\left(1+\tilde{P}\right)\left(\tilde{P}+\widetilde{V_p}+\tilde{P}\widetilde{V_p}\right)} \tag{A1}$$

where $\tilde{P}$ is rescaled precipitation and $\widetilde{V_p}$ is the rescaled vapourization potential at the mean annual scale, calculated as:

$$\tilde{P} = \frac{P-\lambda_s W_p}{\left(1-\lambda_s\right)W_p} \tag{A2}$$

$$\widetilde{V_p} = \frac{V_p-\lambda_u V_p}{\left(1-\lambda_s\right)W_p} \tag{A3}$$

$\widetilde{V_p}$ / $\tilde{P}$ can be called rescaled aridity index. From Equation A1, it can be seen that BFC is jointly controlled by $\tilde{P}$ and $\widetilde{V_p}$, thereby synthesizing the controls of precipitation and four parameters. The four parameters are wetting potential (W_p), evapotranspiration potential (V_p), surface flow abstraction (λ_s), and baseflow initial abstraction (λ_u).

Data Availability Statement

Data of Australia catchments are part of the Australia unregulated catchment data set (Y. Zhang et al., 2013). Data of the conterminous United States catchments are obtained from the Model Parameter Estimation Experiment (MOPEX) data set (Duan et al., 2006). For catchments from United Kingdom, catchment boundaries and daily streamflow data are obtained from UK Benchmark Network (UKBN2) (Harrigan et al., 2018), on the website of National River Flow Archive (https://nrfa.ceh.ac.uk/benchmark-network). Daily precipitation data are obtained from the Center for Ecology & Hydrology (https://catalogue.ceh.ac.uk/documents/33604ea0-c238-4488-813d-0ad9ab7c51ca) (Tanguy et al., 2016). Daily potential evapotranspiration data are obtained from the Climate Hydrology and Ecology Research Support System–Potential Evapotranspiration (GHESS-PE) (http://nora.nerc.ac.uk/id/eprint/516155) (E. Robinson et al., 2016).

Acknowledgments
This study was supported by the National Natural Science Foundation of China (51961145104; 51879193; 41890822); the National Key Research and Development Program of China (2018YFC0407202); and the Overseas Expertise Introduction Project for Discipline Innovation (111 Project) funded by the Ministry of Education and the State Administration of Foreign Experts Affairs P. R. China (B18037).

References

Abatzoglou, J. T., & Ficklin, D. L. (2017). Climatic and physiographic controls of spatial variability in surface water balance over the contiguous United States using the Budyko relationship. *Water Resources Research*, *53*(9), 7630–7643. https://doi.org/10.1002/2017wr020843

Ahiablame, L., Chaubey, I., Engel, B., Cherkauer, K., & Merwade, V. (2013). Estimation of annual baseflow at ungauged sites in Indiana USA. *Journal of Hydrology*, *476*, 13–27. https://doi.org/10.1016/j.jhydrol.2012.10.002

Ahiablame, L., Sheshukov, A. Y., Rahmani, V., & Moriasi, D. (2017). Annual baseflow variations as influenced by climate variability and agricultural land use change in the Missouri River Basin. *Journal of Hydrology*, *551*, 188–202. https://doi.org/10.1016/j.jhydrol.2017.05.055

Ayers, J. R., Villarini, G., Jones, C., & Schilling, K. (2019). Changes in monthly baseflow across the U.S. Midwest. *Hydrological Processes*, *33*(5), 748–758. https://doi.org/10.1002/hyp.13359

Beck, H., van Dijk, A., Miralles, D., de Jeu, R., Bruijnzeel, L. A., Mcvicar, T., & Schellekens, J. (2013). Global patterns in base flow index and recession based on streamflow observations from 3394 catchments. *Water Resources Research*, *49*, 7843–7863. https://doi.org/10.1002/2013wr013918

Bloomfield, J. P., Allen, D. J., & Griffiths, K. J. (2009). Examining geological controls on baseflow index (BFI) using regression analysis: An illustration from the Thames Basin, UK. *Journal of Hydrology*, *373*(1), 164–176. https://doi.org/10.1016/j.jhydrol.2009.04.025

Brandes, D., Hoffmann, J. G., & Mangarillo, J. T. (2005). Base flow recession rates, low flows, and hydrologic features of small watersheds in Pennsylvania, USA. *Journal of the American Water Resources Association*, *41*(5), 1177–1186. https://doi.org/10.1111/j.1752-1688.2005.tb03792.x

Budyko, M. I. (1958). *The heat balance of the earth's surface*. US Department of Commerce.

Budyko, M. I. (1974). *Climate and life* (p. 508). Academic Press.

Calder, I. R. (1998). Water use by forests, limits and controls. *Tree Physiology*, *18*(8–9), 625–631. https://doi.org/10.1093/treephys/18.8-9.625

Cheng, L., Xu, Z., Wang, D., & Cai, X. (2011). Assessing interannual variability of evapotranspiration at the catchment scale using satellite-based evapotranspiration data sets, *Water Resources Research*, *47*, W09509. https://doi.org/10.1029/2011WR010636

Cheng, L., Yaeger, M., Viglione, A., Coopersmith, E., Ye, S., & Sivapalan, M. (2012). Exploring the physical controls of regional patterns of flow duration curves - Part 1: Insights from statistical analyses. *Hydrology and Earth System Sciences*, *16*(11), 4435–4446. https://doi.org/10.5194/hess-16-4435-2012

Cheng, L., Zhang, L., & Brutsaert, W. (2016). Automated selection of pure base flows from regular daily streamflow data: Objective algorithm, *Journal of Hydrologic Engineering*, *21*(11), 06016008. https://doi.org/10.1061/(ASCE)HE.1943-5584.0001427

Cheng, L., Zhang, L., Chiew, F. H. S., Canadell, J. G., Zhao, F., Wang, Y.-P., et al. (2017). Quantifying the impacts of vegetation changes on catchment storage-discharge dynamics using paired-catchment data. *Water Resources Research*, *53*(7), 5963–5979. https://doi.org/10.1002/2017wr020600

Cheng, S., Cheng, L., Liu, P., Zhang, L., Xu, C., Xiong, L., & Xia, J. (2020). Evaluation of baseflow modelling structure in monthly water balance models using 443 Australian catchments. *Journal of Hydrology*, *591*, 125572. https://doi.org/10.1016/j.jhydrol.2020.125572

Daly, E., Calabrese, S., Yin, J., & Porporato, A. (2019). Hydrological spaces of long-term catchment water balance. *Water Resources Research*, *55*(12), 10747–10764. https://doi.org/10.1029/2019wr025952

Donohue, R. J., Roderick, M. L., & McVicar, T. R. (2012). Roots, storms and soil pores: Incorporating key ecohydrological processes into Budyko's hydrological model. *Journal of Hydrology*, *436–437*, 35–50. https://doi.org/10.1016/j.jhydrol.2012.02.033

Duan, Q., Schaake, J., Andreassian, V., Franks, S., Goteti, G., Gupta, H. V., et al. (2006). Model Parameter Estimation Experiment (MOPEX): An overview of science strategy and major results from the second and third workshops. *Journal of Hydrology*, *320*(1–2), 3–17. https://doi.org/10.1016/j.jhydrol.2005.07.031

Fan, Y., Li, H., & Miguez-Macho, G. (2013). Global patterns of groundwater table depth. *Science*, *339*(6122), 940–943. https://doi.org/10.1126/science.1229881

Farnsworth, R., Thompson, E., & Peck, E. (1982). *Evaporation atlas for the contiguous 48 United States* (NOAA technical report, NWS 33). U. S. Department of Commerce.

Ficklin, D. L., Robeson, S. M., & Knouft, J. H. (2016). Impacts of recent climate change on trends in baseflow and stormflow in United States watersheds. *Geophysical Research Letters*, *43*(10), 5079–5088. https://doi.org/10.1002/2016gl069121

Fu, B. F. (1981). On the calculation of the evaporation from land surface. *Chinese Journal of Atmospheric Sciences*, *5*(1), 23–31. (in Chinese).

Gebert, W. A., Radloff, M. J., Considine, E. J., & Kennedy, J. L. (2007). Use of streamflow data to estimate base Flow/groundwater recharge for Wisconsin. *Journal of the American Water Resources Association*, *43*(1), 220–236. https://doi.org/10.1111/j.1752-1688.2007.00018.x

Gentine, P., D'Odorico, P., Lintner, B., Sivandran, G., & Salvucci, G. (2012). *Interdependence of climate, soil, and vegetation as constrained by the Budyko curve* (p. 19404).

Gnann, S. J., Woods, R. A., & Howden, N. J. K. (2019). Is there a baseflow Budyko curve? *Water Resources Research*, *55*(4), 2838–2855. https://doi.org/10.1029/2018wr024464

Good, S. P., Moore, G. W., & Miralles, D. G. (2017). A mesic maximum in biological water use demarcates biome sensitivity to aridity shifts. *Nature Ecology & Evolution*, *1*(12), 1883–1888. https://doi.org/10.1038/s41559-017-0371-8

Grefenstette, J. J. (1986). Optimization of control parameters for genetic algorithms. *IEEE Transactions on Systems, Man, and Cybernetics*, *16*(1), 122–128. https://doi.org/10.1109/tsmc.1986.289288

Hahm, W. J., Dralle, D. N., Rempe, D. M., Bryk, A. B., Thompson, S. E., Dawson, T. E., & Dietrich, W. E. (2019). Low subsurface water storage capacity relative to annual rainfall decouples mediterranean plant productivity and water use from rainfall variability. *Geophysical Research Letters*, *46*(12), 6544–6553. https://doi.org/10.1029/2019gl083294

Hahm, W. J., Rempe, D. M., Dralle, D. N., Dawson, T. E., Lovill, S. M., Bryk, A. B., et al. (2019). Lithologically controlled subsurface critical zone thickness and water storage capacity determine regional plant community composition. *Water Resources Research*, *55*(4), 3028–3055. https://doi.org/10.1029/2018wr023760

Hall, F. R. (1968). Base-flow recessions—A review. *Water Resources Research*, *4*(5), 973–983. https://doi.org/10.1029/wr004i005p00973

Han, J., Yang, Y., Roderick, M. L., McVicar, T. R., Yang, D., Zhang, S., et al. (2020). Assessing the steady-state assumption in water balance calculation across global catchments. *Water Resources Research*, *56*(7). e2020WR027392. https://doi.org/10.1029/2020WR027392

Harman, C. J., Troch, P. A., & Sivapalan, M. (2011). Functional model of water balance variability at the catchment scale: 2. Elasticity of fast and slow runoff components to precipitation change in the continental United States, *Water Resources Research*, *47*(2). W02523. https://doi.org/10.1029/2010WR009656

Harrigan, S., Hannaford, J., Muchan, K., & Marsh, T. J. (2018). Designation and trend analysis of the updated UK Benchmark Network of river flow stations: The UKBN2 dataset. *Hydrology Research*, *49*(2), 552–567. https://doi.org/10.2166/nh.2017.058

Huseby Karlsen, R., Grabs, T., Bishop, K., Buffam, I., Laudon, H., & Seibert, J. (2016). Landscape controls on spatiotemporal discharge variability in a boreal catchment. *Water Resources Research*, *52*(8), 6541–6556. https://doi.org/10.1002/2016wr019186

Jolánkai, Z., & Koncsos, L. (2015). Base flow index estimation on gauged and ungauged catchments in Hungary using digital filter, multiple linear regression and artificial neural networks. *Periodica Polytechnica: Civil Engineering*, *62*(2), 363–372.

Kelly, L., Kalin, R. M., Bertram, D., Kanjaye, M., Nkhata, M., & Sibande, H. (2019). Quantification of temporal variations in base flow index using Sporadic River data: Application to the Bua catchment, Malawi. *Water*, *11*(5), 901. https://doi.org/10.3390/w11050901

Longobardi, A., & Villani, P. (2008). Baseflow index regionalization analysis in a mediterranean area and data scarcity context: Role of the catchment permeability index. *Journal of Hydrology*, *355*(1), 63–75. https://doi.org/10.1016/j.jhydrol.2008.03.011

Lvovich, M. I. (1979). *World water resources and their future* (p. 415).

Lyne, V., & Hollick, M. (1979). *Stochastic time-variable rainfall-runoff modelling* (p. 89–93). Institute of Engineers Australia.

Male, J. W., & Ogawa, H. (1984). Tradeoffs in water-quality management. *Jounal of Water Resources Planning and Managemet-ASCE*, *110*(4), 434–444. https://doi.org/10.1061/(asce)0733-9496(1984)110:4(434)

Mcdonnell, J. J., Sivapalan, M., Vaché, K., Dunn, S., Grant, G., Haggerty, R., et al. (2007). Moving beyond heterogeneity and process complexity: A new vision for watershed hydrology, *Water Resources Research*, *43*(7), W07301. https://doi.org/10.1029/2006wr005467

McNamara, J. P., Tetzlaff, D., Bishop, K., Soulsby, C., Seyfried, M., Peters, N. E., et al. (2011). Storage as a metric of catchment comparison. *Hydrological Processes*, *25*(21), 3364–3371. https://doi.org/10.1002/hyp.8113

Milly, P. C. D. (1994). Climate, soil water storage, and the average annual water balance. *Water Resources Research*, *30*(7), 2143–2156. https://doi.org/10.1029/94wr00586

Nash, J. E., & Sutcliffe, J. V. (1970). River flow forecasting through conceptual models, Part I—A discussion of principles. *Journal of Hydrology*, *10*, 282–290. https://doi.org/10.1016/0022-1694(70)90255-6

Nathan, R. J., & McMahon, T. A. (1990). Evaluation of automated techniques for base flow and recession analyses. *Water Resources Research*, *26*(7), 1465–1473. https://doi.org/10.1029/wr026i007p01465

Neto, M., Roy, T., de Oliveira, P. T. S., & Troch, P. A. (2020). An aridity index-based formulation of streamflow components. *Water Resources Research*, *56*(9), e2020WR027123. https://doi.org/10.1029/2020wr027123

NRFA. (2019). Retrieved from https://nrfa.ceh.ac.uk

Pan, Z., Liu, P., Xu, C. Y., Cheng, L., Tian, J., Cheng, S., & Xie, K. (2020). The influence of a prolonged meteorological drought on catchment water storage capacity: A hydrological-model perspective. *Hydrology and Earth System Sciences*, *24*(9), 4369–4387. https://doi.org/10.5194/hess-24-4369-2020

Peña-Arancibia, J. L., Van Dijk, A. I. J. M., Mulligan, M., & Bruijnzeel, L. A. (2010). The role of climatic and terrain attributes in estimating baseflow recession in tropical catchments. *Hydrology and Earth System Sciences*, *14*(11), 2193–2205. https://doi.org/10.5194/hess-14-2193-2010

Penman, H. (1948). Natural evaporation from open water, bare soil and grass. *Proceedings of the Royal Society A: Mathematical, Physical and Engineering Sciences*, *193*, 120–145. https://doi.org/10.1098/rspa.1948.0037

Poff, L. R., Allan, J. D., Bain, M. B., Karr, J. R., Prestegaard, K. L., Richter, B. D., et al. (1997). The natural flow regime. *BioScience*, *47*(11), 769–784. https://doi.org/10.2307/1313099

Ponce, V. M., & Shetty, A. V. (1995). A conceptual model of catchment water balance: 1. Formulation and calibration. *Journal of Hydrology*, *173*(1), 27–40. https://doi.org/10.1016/0022-1694(95)02739-c

Potter, N. J., Zhang, L., Milly, P. C. D., McMahon, T. A., & Jakeman, A. J. (2005). Effects of rainfall seasonality and soil moisture capacity on mean annual water balance for Australian catchments, *Water Resources Research*, *41*(6), W06007. https://doi.org/10.1029/2004WR003697

Price, K. (2011). Effects of watershed topography, soils, land use, and climate on baseflow hydrology in humid regions: A review. *Progress in Physical Geography: Earth and Environment*, *35*(4), 465–492. https://doi.org/10.1177/0309133311402714

Priestley, C., & Taylor, R. (1972). On the assessment of surface heat flux and evaporation using large scale parameters. *Monthly Weather Review*, *100*, 81–92. https://doi.org/10.1175/1520-0493(1972)100<0081:otaosh>2.3.co;2

Robinson, E., Blyth, E., Clark, D., Comyn-Platt, E., Finch, J., & Rudd, A. (2016). *Climate hydrology and ecology research support system potential evapotranspiration dataset for Great Britain (1961–2015) [CHESS-PE]*. NERC-Environmental Information Data Centre. Retrieved from https//doi.org/10.5285/8baf805d-39ce-4dac-b224-c926ada353b7

Robinson, E. L., Blyth, E. M., Clark, D. B., Finch, J., & Rudd, A. C. (2017). Trends in atmospheric evaporative demand in Great Britain using high-resolution meteorological data. *Hydrology and Earth System Sciences*, *21*(2), 1189–1224. https://doi.org/10.5194/hess-21-1189-2017

Roderick, M. L., & Farquhar, G. D. (2011). A simple framework for relating variations in runoff to variations in climatic conditions and catchment properties. *Water Resources Research*, *47*(12), W00G07. https://doi.org/10.1029/2010WR009826

Rumsey, C. A., Miller, M. P., Susong, D. D., Tillman, F. D., & Anning, D. W. (2015). Regional scale estimates of baseflow and factors influencing baseflow in the Upper Colorado River Basin. *Journal of Hydrology: Regional Studies*, *4*, 91–107. https://doi.org/10.1016/j.ejrh.2015.04.008

Sankarasubramanian, A., & Vogel, R. (2002). Annual hydroclimatology of the United States. *Water Resources Research*, *38*(6), 19-1–19-12. https://doi.org/10.1029/2001wr000619

Shen, Q., Cong, Z., & Lei, H. (2017). Evaluating the impact of climate and underlying surface change on runoff within the Budyko framework: A study across 224 catchments in China. *Journal of Hydrology*, *554*, 251–262. https://doi.org/10.1016/j.jhydrol.2017.09.023

Singh, S. K., Pahlow, M., Booker, D. J., Shankar, U., & Chamorro, A. (2019). Towards baseflow index characterisation at national scale in New Zealand. *Journal of Hydrology*, *568*, 646–657. https://doi.org/10.1016/j.jhydrol.2018.11.025

Sivapalan, M., Yaeger, M. A., Harman, C. J., Xu, X., & Troch, P. A. (2011). Functional model of water balance variability at the catchment scale: 1 Evidence of hydrologic similarity and space-time symmetry. *Water Resources Research*, *47*, W02522. https://doi.org/10.1029/2010WR009568

Smakhtin, V. U. (2001). Low flow hydrology: A review. *Journal of Hydrology*, *240*(3), 147–186. https://doi.org/10.1016/S0022-1694(00)00340-1

Tan, X., Liu, B., & Tan, X. (2020). Global changes in baseflow under the impacts of changing climate and vegetation. *Water Resources Research*, *56*(9), e2020WR027349. https://doi.org/10.1029/2020wr027349

Tang, Y., & Wang, D. (2017). Evaluating the role of watershed properties in long-term water balance through a Budyko equation based on two-stage partitioning of precipitation. *Water Resources Research*, *53*(5), 4142–4157. https://doi.org/10.1002/2016wr019920

Tanguy, M. H. D., Prosdocimi, I., Morris, D. G., & Keller, V. D. J. (2016). *Gridded estimates of daily and monthly areal rainfall for the United Kingdom (1890–2015) [CEH-GEAR]*. Retieved from https//doi.org/10.5285/33604ea0-c238-4488-813d-0ad9ab7c51ca

Trancoso, R., Larsen, J. R., McAlpine, C., McVicar, T. R., & Phinn, S. (2016). Linking the Budyko framework and the Dunne diagram. *Journal of Hydrology*, *535*, 581–597. https://doi.org/10.1016/j.jhydrol.2016.02.017

Trancoso, R., Larsen, J. R., McVicar, T. R., Phinn, S. R., & McAlpine, C. A. (2017). CO_2-vegetation feedbacks and other climate changes implicated in reducing base flow. *Geophysical Research Letters*, *44*(5), 2310–2318. https://doi.org/10.1002/2017gl072759

Van Dijk, A. I. J. M. (2010). Climate and terrain factors explaining streamflow response and recession in Australian catchments. *Hydrology and Earth System Sciences*, *14*(1), 159–169. https://doi.org/10.5194/hess-14-159-2010

Wang, D. (2018). A new probability density function for spatial distribution of soil water storage capacity leads to the SCS curve number method. *Hydrology and Earth System Sciences*, *22*(12), 6567–6578. https://doi.org/10.5194/hess-22-6567-2018

Wang, D., & Hejazi, M. (2011). Quantifying the relative contribution of the climate and direct human impacts on mean annual streamflow in the contiguous United States, *Water Resources Research*, *47*, W00J12. https://doi.org/10.1029/2010WR010283

Wang, D., & Wu, L. (2013). Similarity of climate control on base flow and perennial stream density in the Budyko framework. *Hydrology and Earth System Sciences*, *17*(1), 315–324. https://doi.org/10.5194/hess-17-315-2013

Wu, J., Miao, C., Duan, Q., Lei, X., Li, X., & Li, H. (2019). Dynamics and attributions of baseflow in the semiarid Loess Plateau. *Journal of Geophysical Research: Atmospheres*, *124*(7), 3684–3701. https://doi.org/10.1029/2018jd029775

Xing, W., Wang, W., Shao, Q., & Yong, B. (2018). Identification of dominant interactions between climatic seasonality, catchment characteristics and agricultural activities on Budyko-type equation parameter estimation. *Journal of Hydrology*, *556*, 585–599. https://doi.org/10.1016/j.jhydrol.2017.11.048

Xu, W., Liu, P., Cheng, L., Zhou, Y., Xia, Q., Gong, Y., & Liu, Y. (2021). Multi-step wind speed prediction by combining a WRF simulation and an error correction strategy. *Renewable Energy*, *163*, 772–782. https://doi.org/10.1016/j.renene.2020.09.032

Xu, X., Liu, W., Scanlon, B. R., Zhang, L., & Pan, M. (2013). Local and global factors controlling water-energy balances within the Budyko framework. *Geophysical Research Letters*, *40*(23), 6123–6129. https://doi.org/10.1002/2013gl058324

Yang, D., Sun, F., Liu, Z., Cong, Z., Ni, G., & Lei, Z. (2007). Analyzing spatial and temporal variability of annual water-energy balance in nonhumid regions of China using the Budyko hypothesis. *Water Resources Research*, *43*(4), W04426. https://doi.org/10.1029/2006wr005224

Yokoo, Y., Sivapalan, M., & Oki, T. (2008). Investigating the roles of climate seasonality and landscape characteristics on mean annual and monthly water balances. *Journal of Hydrology*, *357*(3), 255–269. https://doi.org/10.1016/j.jhydrol.2008.05.010

Zhang, J., Zhang, Y., Song, J., & Cheng, L. (2017). Evaluating relative merits of four baseflow separation methods in Eastern Australia. *Journal of Hydrology*, *549*, 252–263. https://doi.org/10.1016/j.jhydrol.2017.04.004

Zhang, L., Dawes, W. R., & Walker, G. R. (2001). Response of mean annual evapotranspiration to vegetation changes at catchment scale. *Water Resources Research*, *37*(3), 701–708. https://doi.org/10.1029/2000wr900325

Zhang, L., Hickel, K., Dawes, W. R., Chiew, F., Western, A. W., & Briggs, P. R. (2004). A rational function approach for estimating mean annual evapotranspiration, *Water Resources Research*, *40*(2), W02502. https://doi.org/10.1029/2003WR002710

Zhang, L., Potter, N., Hickel, K., Zhang, Y., & Shao, Q. (2008). Water balance modeling over variable time scales based on the Budyko framework—Model development and testing. *Journal of Hydrology*, *360*(1–4), 117–131. https://doi.org/10.1016/j.jhydrol.2008.07.021

Zhang, Y., Viney, N., Frost, A., Oke, A., Brooks, M., Chen, Y., et al. (2013). *Collation of Australian modeller's streamflow dataset for 780 unregulated Australian catchments*. Water for a Healthy Country National Research Flagship, CSIRO.